NOVA R & D Inc.
1525 Third St., Suite C
Riverside, CA 92507, USA
www.novarad.com

Tel: 909.781.7332
Fax: 909.781.0178
nova@novarad.com

Image Quality Of A Prototype Direct Conversion Detector For Digital Mammography

James G. Mainprize, Nancy L. Ford, Shi Yin, Tumay Tumer, Martin J. Yaffe
Imaging/Bioengeering Research, Sunnybrook & Women's College Health Sciences Centre, University of Toronto, Toronto, Canada
Nova R & D, Riverside, California, U.S.A.

Image Quality Of A Prototype Direct Conversion Detector For Digital Mammography

James G. Mainprize[a], Nancy L. Ford[a], Shi Yin[b], Tümay Tümer[b], Martin J. Yaffe[a]

[a]Imaging/Bioengeering Research, Sunnybrook & Women's College Health Sciences Centre, University of Toronto, Toronto, Canada

[b]Nova R & D, Riverside, California, U.S.A.

ABSTRACT

A digital mammography system in which the x-ray sensitive device is a solid-state direct conversion detector is under development. This detector is a 1 mm thick silicon photodiode array hybridized to a CCD read-out, with a 50 μm pixel pitch. The detector is designed to be used in a slot-scanned system using time-delay integration (TDI) for signal acquisition. To handle the large signal generated in the photodiode, a novel read-out technique was used, in which charge was integrated "on-chip" over a small number of rows, and the output of each of these sections was digitally summed "off-chip" to produce the total integrated signal for each pixel in the image. This two-stage integration process not only allows easy acquisition of large signals, it effectively increases bit depth from 12 bits (for a single section) to approximately 16 (for the total integrated signal). The image quality of the device has been measured and compared to predictions based on cascaded linear systems theory. The resolution of the new detector was determined from the modulation transfer function (MTF) which was obtained from over-sampled edge spread functions (ESF). The ESF was measured in both the scan and slot directions from four repeated images of a tantalum edge. Noise power spectra (NPS) were determined from 40 repeated flat-field images at each of several x-ray exposures. By combining the MTF and NPS measurements, the detective quantum efficiency (DQE) was also determined. The MTF in the non-scanned direction was found to >20% at 10 mm^{-1} and slightly lower in the scanned direction ($\approx$ 10% at 10 mm^{-1}). In all cases, the DQE was at least comparable to film-screen mammography receptors. The DQE at 120 mR detector exposure at zero spatial frequency ranged from 0.4 to 0.6 depending on the sample tested. Electronic noise was fairly low, contributing to less than $\pm$7 ADU (out of a possible 98304 ADU). Future work will involve re-designing the prototype to use a photoconductor with higher density and atomic number to improve quantum interaction efficiency and reduce geometric constraints on image quality.

Keywords: x-ray detector, CCD, silicon, photodiode, DQE, digital mammography

1. INTRODUCTION

Digital mammography has several potential advantages over conventional film-screen techniques. Several types of detectors have been proposed and there are several systems undergoing clinical approval. Most of these systems are based on a phosphor coupled to a light-sensitive detector. These devices do have some limitations, including a poor energy conversion efficiency of the phosphor, low coupling efficiency between the phosphor and the detector, and blurring introduced by light diffusion in the phosphor. As a result, these systems tend to have a resolution that is poorer than screen-film and a DQE that is only slightly better.

Alternatively, a direct conversion detector can be used. These detectors absorb x rays and convert this energy directly into an electronic charge signal. An applied electric field across these detectors enhances signal collection and reduces lateral spread of charge. Because there is almost no blurring of the charge signal, these detectors can be made very thick to provide nearly 100% quantum interaction efficiency.

In this work we describe the initial measurements of image quality on a novel direct conversion detector for mammography.

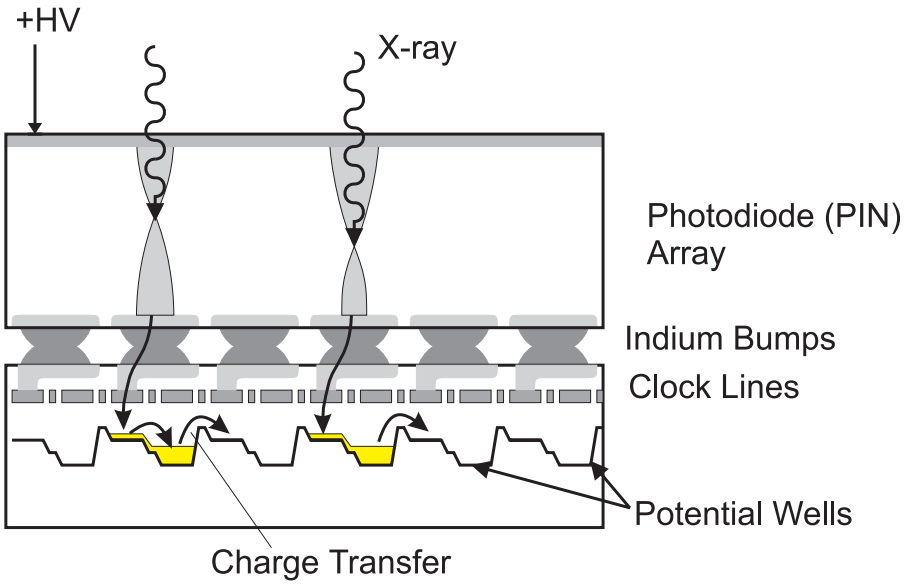

Figure 1. Cross section of the hybrid detector. Liberated charges produced by absorption of an x ray are swept to the electrodes on the PIN diode. Charge is transferred to the CCD by the indium bump bonds, and transferred down a column as a charge packet by controlling the clocking gates in the CCD.

2. PROTOTYPE DETECTOR

The prototype detector is a hybrid device which consists of a photodiode array bonded to a CCD for charge collection and read-out (Figure 1). In the prototype, a 1.0 mm thick Si crystalline P-I-N photodiode array was used.

Each photodiode array element is attached to a CCD cell by an indium bump-bond. The CCD is operated in time delay integration (TDI) mode, in which the device is scanned at a constant velocity in one direction, and charge transfer through the CCD occurs at an equal speed but in the opposite direction.

Silicon has a very high conversion gain producing about 5500 electron-hole pairs (EHP) for a 20 keV x-ray (or 3.6 eV/EHP). This provides excellent signal levels that are substantially higher than the predicted electronic noise. However, the total number of EHPs required per pixel in a mammographic image does pose a problem. The detector must be able to accommodate the largest signal which can be 1000 mR or more in mammography. This corresponds to 1.38×10^5 x rays, or 7.6×10^8 EHPs for each pixel in the image. Unfortunately CCD well capacity is quite limited, with maximum charge storage levels about an order of magnitude lower ($\approx 10^7$ EHPs) than required.

To accommodate the large signals, a novel read-out design was developed, in which the TDI was performed in two stages (Figure 2). The CCD consists of 24 sections, with 8 TDI stages per section. Normal "on-chip" integration is performed in each of these stages. Then the signal is transferred "off-chip" and the signal from each of the 24 sections is combined together, with the correct timing delay between each section.

Since there are 24 sections combining together to yield an image, each CCD well only needs to hold 3.2×10^7 EHPs which is much easier to achieve with existing CCD technology.

3. THEORETICAL IMAGE QUALITY

The image quality of the detector was compared to a theoretical predication of image quality based on a cascaded linear systems analysis. In this type of analysis, the imaging chain is described by one of five processes: gain, stochastic blurring, deterministic blurring, noise addition, or aliasing. For example, the signal spectrum, $S(f)$, and noise power spectrum, $NPS(f)$, transfer through a stochastic blurring stage, i, as follows:

$$S_i(f) = MTF(f) S_{i-1}(f), \quad (1)$$

$$NPS_i(f) = MTF^2(f) \left(NPS_{i-1} - \Phi_{i-1}\right) + \Phi_{i-1}, \quad (2)$$

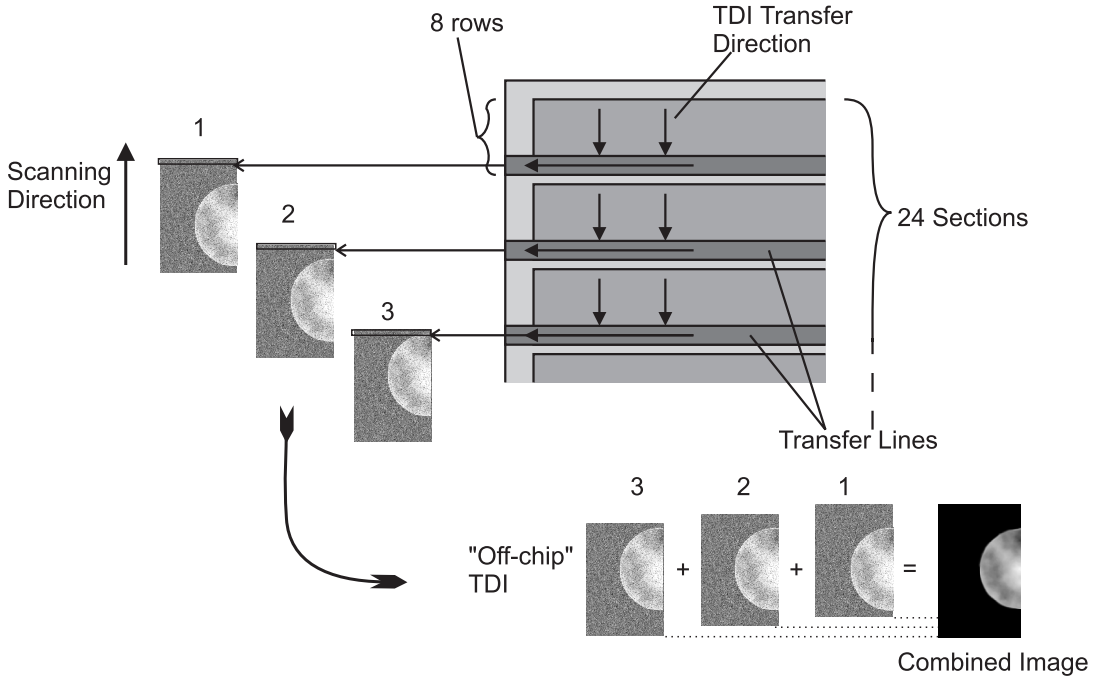

Figure 2. Schematic of the novel two-stage TDI process. The detector is divided into 24 sections, each of which performs normal TDI over 8 rows. The charge signal is transferred off-chip and integrated together with appropriate delays between each section. This figure is not to scale.

where Φ_{i-1} is the fluence from the previous stage. The propagation of signal and noise is calculated through each of these stages, and the spatial frequency dependent $DQE(f)$ is determined by calculating the signal to noise ratio (SNR) at the output of the imaging chain and comparing to the ideal input SNR (assumed to be Poisson):

$$DQE(f) = \frac{\frac{S^2(f)}{NPS(f)_{out}}}{\frac{S^2(f)}{NPS(f)_{in}}} = \frac{SNR^2_{out}(f)}{SNR^2_{in}(f)}. \tag{3}$$

The cascaded linear systems model for the prototype scanning detector consists of eight stages (Figure 3). For simplicity, the model assumes a monoenergetic spectrum. Each stage is described briefly in the following sections.

X-ray Absorption

The thickness of the depletion zone in a reversed biased diode determines the x-ray absorption efficiency. One particular advantage of a PIN diode is that nearly the entire thickness of the semiconductor becomes depleted, and is thus sensitive to x-rays.

X-ray absorption is a form of gain stage (or binomial selection) with the gain less than one. This gain is also the quantum efficiency, η

$$\eta = 1 - e^{-\mu L}, \tag{4}$$

where μ is the linear absorption coefficient, and L is the thickness of the PIN diode. For a 20 keV x ray, a 1 mm thick Si-PIN diode provides a quantum efficiency of 64%.

Temporal Aperture Blurring

As the detector scans, the charge is transferred down a row at discrete clock intervals. However, the detector is scanned at a continuous velocity, meaning that each detector element sweeps out a distance equal to the detector element pitch, p, between charge transfers. This causes an additional blur in the scan direction.

$$MTF_{scan}(f) = \mathrm{sinc}(pf). \tag{5}$$

Note that this blurring is in addition to the blurring caused by the physical aperture of each detector element (see *aperture blur*, below).

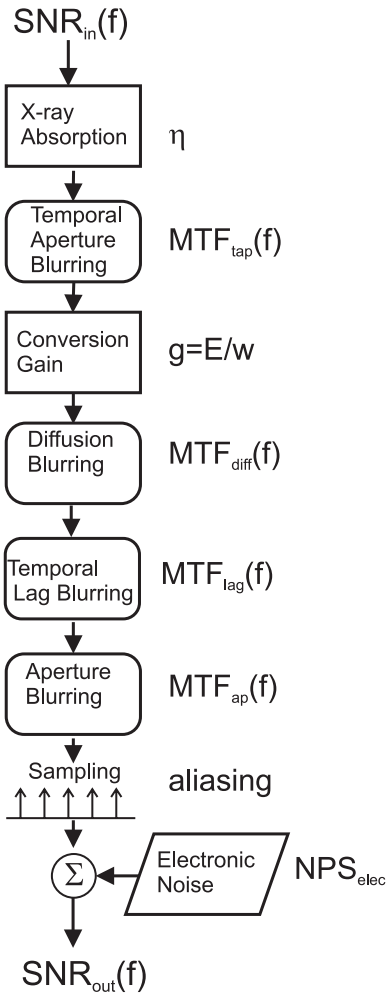

Figure 3. Cascaded linear systems model of the prototype device.

Conversion Gain

When the x ray is absorbed in the PIN diode array, the energy ultimately frees several thousand electron-hole pairs (EHP). As mentioned previously, the energy required, w, to liberate an EHP is 3.6 eV, or a gain of 5500 EHPs per $E = 20$ keV x ray. This conversion gain is stochastic, and has the following signal and noise properties:

$$S_i = gS_{i-1}, \tag{6}$$

$$N_i = g^2 N_{i-1} + \frac{g^2\phi}{1/A_s - 1}. \tag{7}$$

where g is the gain, and A_s is the Swank factor.[1] Since silicon has very good noise properties and since K fluorescence is very low energy, the Swank factor is very close to 1. However, to partially account for the effects of using a polyenergetic spectrum in the experiment, an effective Swank factor of 0.94 was used. This value determined by calculated the spectrally weighted variance in the gain stage for the x-ray spectrum used in the experiments.

Diffusion Blurring

Once the EHPs are liberated, the applied electric field causes the charge carriers to be swept to the opposite surfaces of the diode array. As these charges travel through the detector, they can diffuse laterally, introducing an blur of the form:

$$MTF_{diff}(f) = \frac{\mu\left(e^{-4k_BT(\pi fL)^2/(qV)} - e^{-\mu L}\right)}{\left[\mu - 4k_BT\pi^2 f^2 L/(qV)\right](1 - e^{-\mu L})}, \tag{8}$$

where k_B is Boltzmann's constant, T is the temperature, L is the thickness of the detector, V is the applied bias, and q is the elementary charge.

Temporal Lag Blurring

Charge collection from the photodiode array is not instantaneous. The temporal response, or lag, of the photodiode array will include charge transit times, the effect of charge trapping, and the RC time constant of the detector. In the scanning detector, the lag will produce a blur in the image along the scan direction. If the lag response, $I(t)$ is assumed to be a weighted sum of exponentials of the form:

$$I(t) \propto \sum_{j=1}^{N} \frac{w_j}{\tau_j} e^{-\frac{t}{\tau_j}}, \tag{9}$$

where w_j is the relative weight of the jth component, τ_j is the *lifetime* of the jth component, then the resultant blur will be of the form:

$$MTF_{lag}(f) = \left| \sum_{j=1}^{N} \frac{w_j}{1 + 2\pi i \tau_j v f} \right|. \tag{10}$$

Aperture Blurring

The resolution of a semiconductor detector is governed by sensitive width, w, of each detector element. If the "fill factor" of the detector is 100%, then the sensitive width is equal to the pitch ($w = p$)

$$MTF_{ap}(f) = \mathrm{sinc}(wf). \tag{11}$$

Sampling

Detection in a digital device is ultimately a sampling operation. Sampling causes aliasing, in which high spatial frequency information is reflected down into lower frequencies. Aliasing is a non-linear process and linear systems analysis cannot strictly be used. However, others[2,3] have shown that with certain assumptions, a modified linear systems analysis can be used. In this analysis, it is assumed that the signal is band-limited to the Nyquist frequency (i.e. no aliasing of the signal) which means that the MTF after sampling is simply the pre-sampling MTF. On the other hand, the noise is aliased:

$$N_i(f) = \sum_{k=-\infty}^{\infty} N_{i-1}(f + \frac{k}{p}), \tag{12}$$

where p is the detector element pitch, and $\frac{k}{p}$ represents the harmonic multiple of the sampling frequency. Since the signal is unaffected by aliasing and the low frequency noise is increased due to aliasing, the DQE(f) will drop.

Electronic Noise

The final stage is a noise addition stage, which originates from a variety of sources. These sources include CCD transfer noise, thermal generation of carriers, and amplifier noise. This noise is assumed to be white and is measured experimentally, by taking a "dark" image with no x rays, and determining the variance in the image.

Other Effects

There are several other phenomena that contribute to blurring and noise. These include scanning velocity mismatch and charge transfer inefficiency in the scanning direction, and K fluorescence blurring, and Compton scatter blurring affecting both directions. Their overall effect is small and they are neglected in the calculation.

4. EXPERIMENT

The experimental imaging system is shown in Figure 4. In this setup, the detector chip is held stationary, while the object to be imaged is scanned across it. This particular geometry was chosen for relative simplicity, however, by scanning the object, the scanning velocity must be adjusted for magnification, and thick objects cannot be scanned without significant velocity mismatch blurring.

The tungsten anode tube was operated at 30 kVp and 38 mA, with 0.4 mm Al filtration (mean energy 20.3 keV). The x-ray field was pre- and post- collimated to reduce scatter radiation effects. The detector operated at transfer rate of 1167 lines/s. This corresponds to a scanning velocity of 58.35 mm/s (to accomodate of the small amount of magnification, the object was actually scanned at 56.1 mm/s). The detector was reversed biased to 160-180 V.

The MTF was determined by using a slanted edge technique[4] in both the scan and slot (non-scanned) directions. Each MTF was determined from 4 repeated images of a uniform PMMA block (0.64 mm thick) and a tantalum edge. The edge was placed on the PMMA block nearest the detector. The noise power spectra (NPS) were measured using

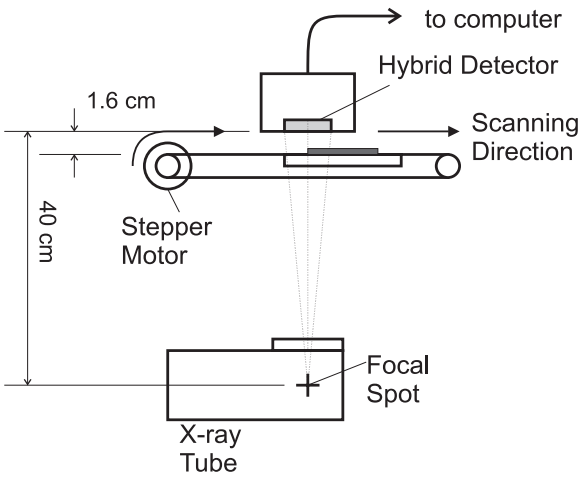

Figure 4. Sketch of the experimental geometry used in the image quality measurements

a simulated slit method[5] from 40 images of the uniform PMMA block. Standard error in the NPS measurement was also determined. The corresponding exposure for each NPS was measured using an ion chamber.

From these measurements, the $DQE(f)$ was determined:

$$DQE(f) = \frac{S^2 MTF^2(f)}{NPS(f) \cdot \Phi}, \tag{13}$$

where S is the mean image signal (in ADU), and Φ is the incident x-ray fluence, determined from the exposure.

The temporal lag of the PIN diode array, was determined in a separate experiment. The lag measurement is similar to phosphor luminescence measurements made by Mainprize and Yaffe[6] in which an x-ray tube is pulsed, and the response of the PIN diode is measured. Using an "iterative deconvolution technique", the lag response is corrected for the arbitrary shape of the original x-ray pulse.

5. RESULTS

The lag time response of the PIN diode array appeared to be best approximated by a three term sum of exponentials. As shown in Table 1, the longest component had a lifetime, τ, of 368 μs which is on the order of the line transfer rate of the CCD, and expected to induce a small amount of blurring in the scan direction.

Lifetime, τ (μs)	368	50	6
Relative weight, w	20%	42%	38%

Table 1. Lag response coefficients for Equation 10

The first detector tested had an unusually large dark current which permitted using only low bias voltage (<160 V), and only functioned for a short time before failure. However, its response was very good while it functioned. Two other detectors (#2, and #3) have been tested. Most of the testing was performed on detector #3, which has been in operation for the longest time. Both detectors had better dark currents and could be biased to slightly higher levels (170-180 V).

All of the relevant parameters for the linear systems model are provided in Table 2.

The MTFs for detector #3 are shown in Figure 5 and are compared to the theoretical MTF based on the cascaded linear systems model. As predicted by the model, the MTF in the scan direction is lower than the slot direction. However, the experimental MTFs are lower than predicted.

Parameter	Value
Detector element width, w	50 μm
Detector element pitch, p	50 μm
Detector thickness, L	1 mm
Dark Noise	$\pm$7 ADU (or $\pm$60000 electrons/pixel)
Mean X-ray Energy, E	20.1
Quantum Efficiency, η	0.64
Operating Temperature, T	300 K
Bias Voltage, V	#1: 160 V, #2: 170 V, #3: 180 V

Table 2. Parameters used in image quality model

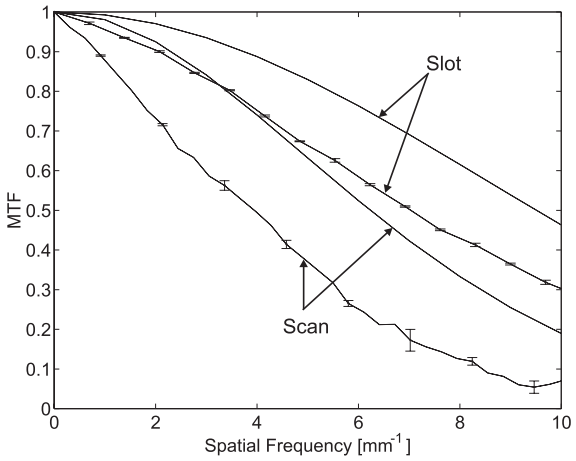

Figure 5. Comparison of theoretical and experimental MTF

The DQE curves of detector #1 and #2 are shown in Figure 6, and appears to agree reasonably well with theory.

The $DQE(f)$ for the third detector was measured at 3 different exposure levels: 126 , 58, and 10 mR (at the detector). Results for the slot and scan directions are shown in Figure 7.

6. DISCUSSION

The experimental $DQE(f)$ appears to be about 25% (at 0 mm^{-1}) lower than predicted. Since the $DQE(f)$ varies little with exposure, the reduction is not due to electronic noise. A possible source of this loss may be due to poor charge collection. Bias voltages have been limited to less than 200 V by excessive dark current levels, which may be affecting charge collection efficiency. Future detector designs have modified guard ring structures to help reduce dark current and higher biases should be possible. Charge collection can also be reduced by incomplete depletion in the photodiode, or by poor electronic coupling between the diode array and the CCD. The detector element "fill factor" may also be causing the DQE reduction.

There is a similar discrepancy in the theoretical and experimental $MTF(f)$. There appears to be an additional blurring mechanism affecting both the scan and slot directions. This mechanism may be related to poor charge collection, or to surface current effects on the photodiode array.

It is important to note that while early results are lower than expected, the response is still superior to screen-film. Screen-film DQEs[7] are at best 0.3 at 0 mm^{-1} and drops to less than 0.01 at spatial frequencies higher than 6 mm^{-1} . Future work will involve developing high quantum efficiency hybrid detectors which will potentially improve DQE(0) to greater than 0.9. Thicker PIN diodes (1.5 mm) and alternative photoconductors such as CdZnTe, and PbI_2 will be investigated.

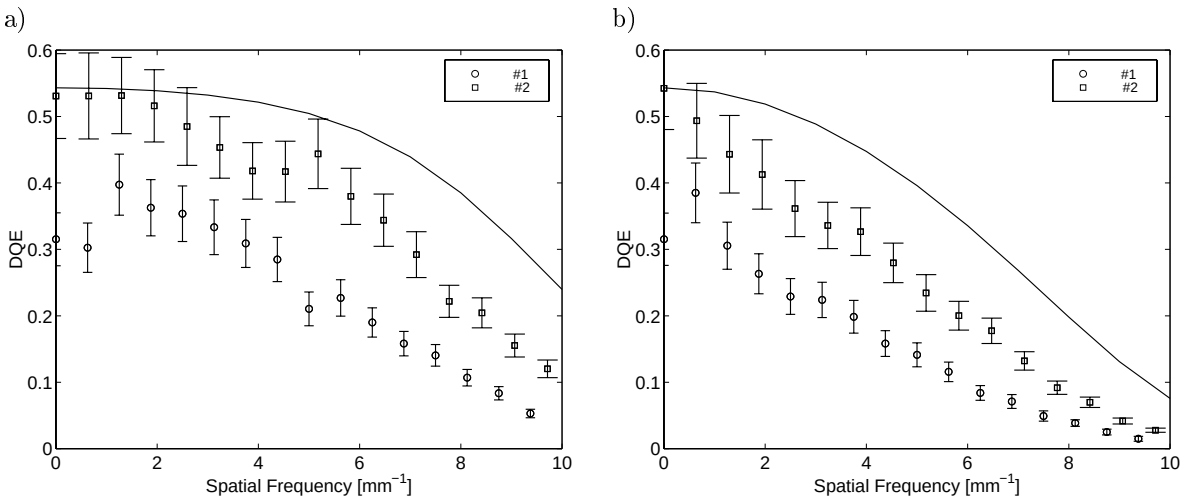

Figure 6. DQE results for detector #1 and #2 in the slot (a) and scan (b) directions. High dark currents ultimately caused the first detector to fail. The second detector is still in operation.

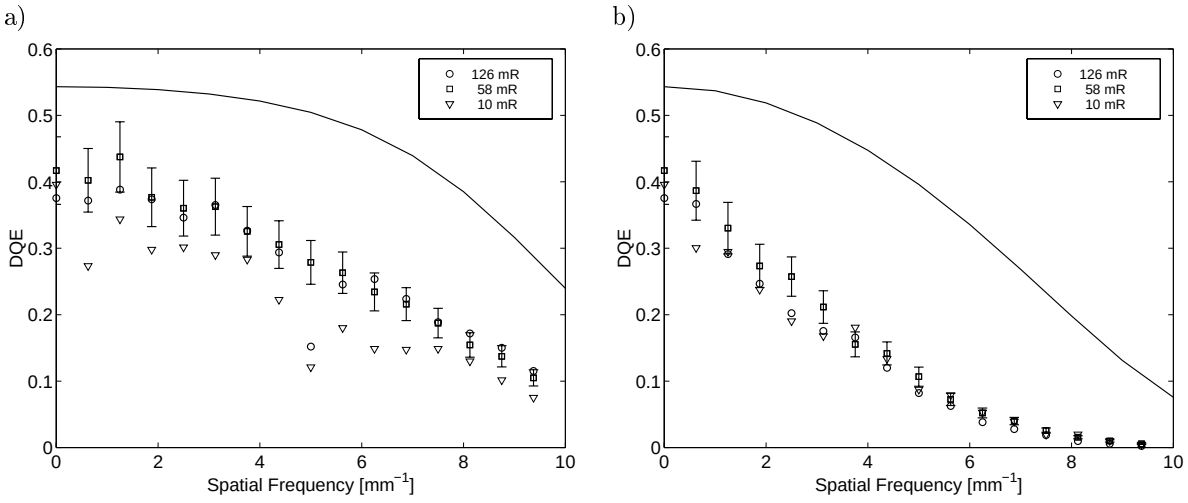

Figure 7. DQE in the slot (a) and scan (b) directions for detector #3. Experimental results at three detector exposures are shown, and the theoretical prediction based on the cascaded model presented in Section 3. Error bars are shown on a single curve for clarity.

7. CONCLUSION

A prototype direct conversion detector has been developed. Early results have demonstrated DQEs higher than screen film over over an exposure range of 10 to 120 mR to the detector. Comparison of the experimental image quality results to a cascaded linear systems model shows similar trends in resolution and DQE. However, the measured results are lower than predicted. Future work will attempt to determine the source of image quality degradation and the detector design will be modified to correct the loss. This prototype has demonstrated the feasibility of a direct conversion slot scanned mammography detector.

REFERENCES

1. R. K. Swank, "Absorption and noise in x-ray phosphors," *J. Appl. Phys.* **44**(9), pp. 4199–4203, 1973.
2. I. A. Cunningham, "Degradation of the detective quantum efficiency due to a non-unity fill factor," *Proc SPIE* **3032**, pp. 22–31, 1997.
3. W. Zhao and J. A. Rowlands, "Digital radiology using active matrix readout of amorphous selenium: Theoretical analysis of detective quantum efficiency," *Med. Phys.* **24**(12), pp. 1819–1833, 1997.
4. P. F. Judy, "The line spread function and modulation transfer function of a computed tomographic scanner," *Medical Physics* **3**(4), pp. 233–236, 1976.
5. J. C. Dainty and R. Shaw, *Image Science*, Academic Press, 1974.
6. J. G. Mainprize and M. J. Yaffe, "The effect of phosphor persistence on image quality in digital x-ray scanning systems," *Medical Physics* **25**(12), pp. 2440–2454, 1998.
7. P. Bunch, "Analysis of the detective quantum efficiency of a radiographic screen-film combination," *Journal of the Optical Society of America. A* **4**, pp. 902–9, May 1987.